Vol. 92 No. 6 pp. 2416–2431 ACTA GEOLOGICA SINICA (English Edition) Dec. 2018

Reviews

Wave-Enhanced Sediment-Gravity Flows in Bohai Bay Lacustrine Basin, Eastern China

BAI Chenyang[1, *], YU Bingsong[1], DONG Tianyang[2], HAN Shujun[1], GE Jia[3] and ZHU Donglin[4, 5]

1 *School of Geosciences and Resources, China University of Geosciences (Beijing), Beijing 100083, China*
2 *Department of Earth, Environmental, and Planetary Sciences, Rice University, Houston, Texas 77005, USA*
3 *Oil & Gas Survey, China Geological Survey, Beijing 100083, China*
4 *Bureau of Geophysical Prospecting Inc., China National Petroleum Corp., Zhuozhou 072751, Hebei, China*
5 *Department of Geosciences, University of Texas at Dallas, Richardson, Texas 75080, USA*

Abstract: Sequences of wave-enhanced sediment-gravity flows (WESGFs) have been widely recognized in the marine shelf environment. In this study, we show observations of WESGF deposits in lacustrine settings using well core and thin section data from the Paleogene in the Jiyang sub-basin, Bohai Bay basin, eastern China. The findings of this study include the following: 1) the sequence of WESGFs in the lacustrine basin is similar to that of marine; it consists of three units, MF1 unit: siltstone with basal erosion surface, MF2 unit: silt-streaked claystone, and MF3 unit: silty-mudstone; and 2) prodelta sand sheets are found in the lacustrine WESGF sequence and are classified as the MFd unit: clay-streaked siltstone. However, because the system size and variability in hydrodynamic conditions are different between the lacustrine and marine basins, lacustrine WESGFs do appear to have three distinguishable features: 1) the sediment grain size and sand content are slightly higher than those of the marine WESGFs; 2) lacustrine WESGFs may contain prodelta sediments or sedimentary sequences of other types of gravity flows, such as hyperpycnal flows; and 3) the scale of the sedimentary structures for lacustrine WESGFs is smaller. The WESGFs found in the continental lacustrine basin provide a new model for sediment dispersal processes in lake environments and may be helpful to explain and predict the distribution of sandy reservoirs for oil and gas exploration.

Key words: wave-enhanced sediment-gravity flows, sediment transport, lacustrine basin, Shahejie Formation, Bohai Bay basin

1 Introduction

Sediment-gravity flow in a marine setting is an important transport mechanism to disperse sediment from a continental shelf edge to a deep-water basin (Macquaker et al., 2010; Plint, 2014, Harazim and Mcilroy, 2015). Classical field studies of ancient turbidite succession and numerical models of turbidity current showed that gravity flows in a marine setting tend to occur at the continental slope, where both the gradient and sediment supply are sufficient, and gravity-induced turbulence can maintain sediment suspension. (e.g., Bouma, 2000; Postma et al., 2015; Wang et al., 2017). However, within the continental shelf, sediment dispersal, especially transport of mud, is not well understood (Macquaker et al., 2010). This limited understanding is because the slopes of many modern continental shelves are too shallow to produce conventional gravity-driven flow (Nittrouer and Wright, 1994). However, mud deposits are observed on the shelf, so there must be additional driving mechanisms. A new type of mud transport within the continental shelf has been proposed (Friedrichs and Wright, 2004; Traykovski et al., 2007; Macquaker et al., 2010), known as wave-enhanced sediment-gravity flows (WESGFs). For WESGFs, sediment is maintained in suspension via the orbital motion of surface gravity waves, by which such flows can occur at a slope as low as 0.5 m/km (Friedrichs and Wright, 2004). Macquaker et al. (2010) predicted sedimentary structure produced by WESGFs. The

* Corresponding author. E-mail: cheny.bai@cugb.edu.cn

sedimentary structure has been observed in field studies of a marine shelf near the Waipaoa River margin and Poverty Bay (Walsh et al., 2014). Similar sequences have been observed in modern WESGF deposits at the Eel shelf, California and in ancient marine sedimentary successions, such as the Cleveland Ironstone Formation (U.K.) and Mowry Shale (Wyoming) (Macquaker et al., 2010; Plint, 2014). More recently, Plint (2014) conducted a detailed microfacies study in the Dunvegan Formation, western Canada Foreland basin. The additional observation of WESGF sequences from sedimentary records includes the following: outcrops of shallow water deposits from the mid-Telychian (Early Silurian), in Anticosti Island, eastern Canada (Clayer and Desrochers, 2014), Whitby Mudstone Formation (Toarcian, lower Jurassic), a marine shelf deposit, from northeast England (Ghadeer and Macquaker, 2012), and the Lower Ordovician (Tremadocian) Beach Formation in Newfoundland (Harazim and Mcilroy, 2015).

Based on evidence from previous studies, WESGFs have been widely recognized as a marine sediment transport process in a shelf environment. However, there is very limited evidence of WESGFs occurring in a lacustrine environment. The physiographical setting of large shallow lake environments can resemble the slope gradient, water depth and wave condition of continental shelves (Gilbert, 1999; Mao and Xia, 2017; Lv Qiqi et al., 2017). For this reason, it is possible for WESGFs to occur in lacustrine settings. However, the sedimentary sequences between marine and lacustrine WESGFs should be different due to the difference in local hydrodynamic conditions. In this study, we use well core and thin section data from a series of production wells in the Jiyang sub-basin, eastern China, to identity the sedimentary sequences of WESGFs in a lacustrine environment. A large volume of seismic data from the study area revealed a Paleogene rifting formed lake that contains a shallow, low-sloping ramp, imitating the geometry of a continental shelf (Tong Yanming et al., 2008; Feng et al., 2013; Zahid et al., 2016). In the subsequent part of this paper, we describe the sedimentary characteristics of the WESGF sequences and the spatial extent of these sequences and then provide a conceptual deposition model of WESGFs in the lacustrine environment and finally compare this model to its marine counterpart. The sandy body formed by WESGFs may extend the distribution range of sandy reservoirs in lacustrine basins.

2 Geological Setting

Located in the eastern part of north China craton, Bohai bay basin is a complex continental rift basin initiated in the Mesozoic and contains several oil and gas reservoirs (Guo et al., 2010; Zhang Shun et al., 2017; Bai et al., 2018). Jiyang sub-basin is a smaller tectonic unit in the eastern part of the Bohai bay basin (Fig. 1a). The Jiyang sub-basin is consisted of Dongying, Huimin, Zhanhua and Chezhen depressions (Fig. 1b). Wells used in this study are located in these smaller tectonic units of the Boxing and Bonan sags within the larger Bohai bay basin (Figs. 1c–d). Specifically, wells FY1 and F120 are in the Boxing sag (northern part of the Dongying depression), and wells Y633 and L358 are in the Bonan sag (eastern part of the Zhanhua depression) (Figs. 1c–d). The Dongying and Zhanhua depressions are typical half-graben basins. The large normal faults of the two depressions are located at the northern margins and the southern margins are hinged and contain smaller conjugate faults (Fig. 2). Boxing sag is located in the southern margin of the Dongying depression and the Bonan sag is located at the southern edge of the Zhanhua depression (Fig. 2).

The Jiyang sub-basin is infilled with the strata of the Paleozoic (Pz), Mesozoic (Mz), and Cenozoic (Cz). The Cenozoic include Paleogene (E), Neogene (N) and Quaternary (Q) from the bottom upward. The Paleogene and the Neogene were the major filling periods of the Dongying depression. Based on lithology and sedimentary environments, the Paleogene has been divided into the Kongdian (Ek) and the Shahejie (Es) Formations. The Shahejie Formation has been further divided from the bottom upward into four members called the fourth (Es_4), the third (Es_3), the second (Es_2) and the first member (Es_1). Es_3 and Es_4 are the major deposition layers for WESGFs. Es_4 has been sub-divided into two sub-members, the lower sub-member of Es_4 (Es_4-2) and the upper sub-member of Es_4 (Es_4-1), and Es_3 has been sub-divided into three sub-members, the lower sub-member of Es_3 (Es_3-3), the middle sub-member of Es_3 (Es_3-2) and the upper sub-member of Es_3 (Es_3-1) (Feng et al., 2013; Zhu Xiaomin et al., 2015) (Fig. 3).

According to a previously established sequence stratigraphic framework, the Jiyang sub-basin is classified into 1st-, 2nd- and 3rd-order sequences (Fig. 3). Sequence boundaries are recognized based on interpretations of 2-D and 3-D seismic, well-log and core data (Feng et al., 2013; Zahid et al., 2016). In Shahejie Formation, there are two hiatuses, representing a period of erosion or non-deposition, and these hiatuses form two 2nd unconformities (between Es_3 and Es_4; between Es_1 and Es_2).

The Es_4-2 contains red sandy mudstone with gypsum salt layers and is interpreted to be indicative of a river floodplain environment. The Es_4-1 is interpreted as delta deposits that contain gray glutenite and thin layers of mudstone (Guo et al., 2012; Feng et al., 2013; Hao et al.,

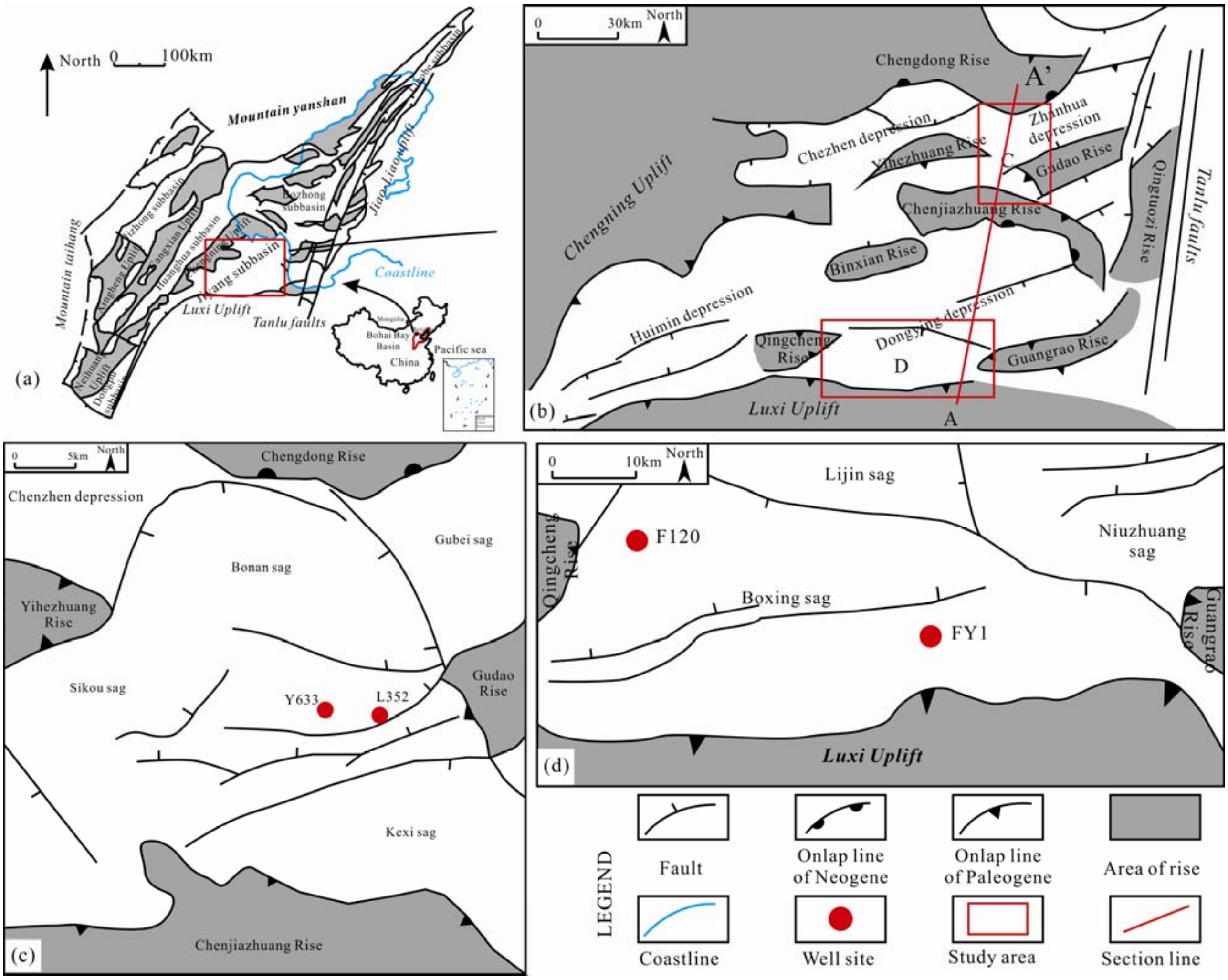

Fig. 1. Tectonic sketch map of study area (modified from Feng et al., 2013).

(a), Structural map of the Bohai bay basin. Red box outlines the Jiyang sub-basin (modified from Feng et al., 2013); (b), structural map of the Jiyang sub-basin. Red box outlines the major study areas. Letter C denotes the approximate location of the Boxing sag in Dongying depression and letter D denotes the approximate location of the Bonan sag in Zhanhua depression. See Fig. 2 for detailed cross-section of A-A' (modified from Feng et al., 2013); (c), structural map of the Boxing sag, where studied wells FY1 and F120 are located at (modified from Geological Scientific Research Institute, Shengli Oilfield Company of SINOPEC, 2008); (d), structural map of the Bonan sag, where studied Wells Y633 and L358 are located at (modified from Geological Scientific Research Institute, Shengli Oilfield Company of SINOPEC, 2008).

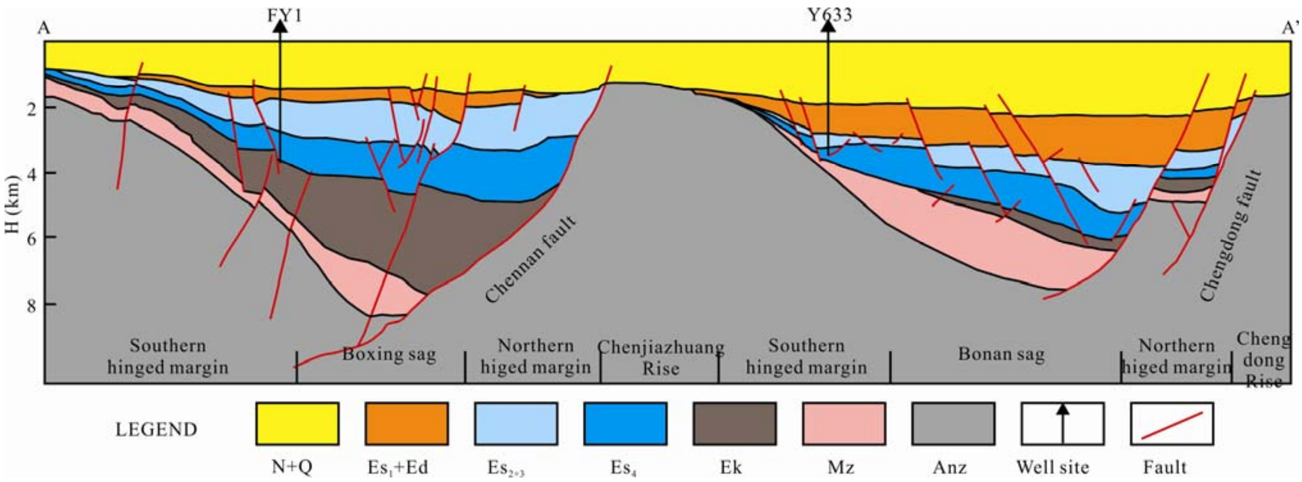

Fig. 2. Cross-section of A-A' from Fig. 1 in the Jiyang sub-basin (modified from Feng, et al., 2013).

2014) (Fig. 3). The depositional environment of Es_3-3 is interpreted as a gradual-transitional deep lacustrine system, by which the major lithologies consist of light-gray mudstone, mud limestone and siltstone. The Es_3-2 contains multiple sets of carbonate layers within mudstone and more sandstone and siltstone than the Es_3-3. The Es_3-1 contains dark mudstone and some siltstone (Guo et al., 2012; Feng et al., 2013; Hao et al., 2014; Wang Jian et al., 2017) (Fig. 3). As previously mentioned, the WESGF sediment samples come from the Es_3-2 to Es_4-1, by which the lake level varied from low to high at this time.

3 Material and Methods

The thickness of these core intervals varies from 2 to 20 cm. The adjacent rocks of these core intervals are mainly mudrock. For the analysis conducted in this study, we focus on these intervals of intensive sand/silt laminae.

The core samples used in this study are from seven different sample intervals in wells FY1, F120, Y633 and L358 (Fig. 3). All seven sample intervals mainly consist of sandstone, siltstone and mudstone. In addition, there are few conglomerate, calcareous mudstone, limestone and dolomite within the sample intervals (Fig. 4 and Table 1).

Thin sections are produced from each of the sediment core interval samples with the following procedures: 1) core samples are cut into rules and flake samples at a size of 20 mm×10 mm×5 mm. 2) The samples are then polished with a rock grinder to remove surface roughness. 3) The samples are further polished manually with a flannelette cloth while applying 1.0 and 3.0 μm alumina slurry polishing liquid. 4) After polishing, samples are cleaned by ultrasonication to further remove impurities. The dried samples are preheated and then coated with epoxy resin. 5) Step 2 is then repeated, and the samples are ground to 0.03 mm thickness and then polished. All polished thin sections are produced in the State Key Laboratory of Geological Processes and Mineral Resources, China University of Geoscience (Beijing) following the above procedures.

4 Petrological Characteristics

4.1 Microfacies division

The core intervals with intensive sand/silt laminae in the study area can be divided into three units, from bottom to top, as MF1, MF2 and MF3, based on lithology and sedimentary structure using methods from previous research (Macquaker et al., 2010; Denommee et al., 2016). MF1 unit is mainly composed of fine sandstone and siltstone, with low mud content; MF2 unit is mainly composed of interbedded silt- and clay-rich layers; and MF3 unit is mainly structureless and composed of clay particles (Fig. 5). There is an additional unit, MFd, observed in the core samples, which is similar to MF2. Detailed descriptions of these four units based on observations from core and thin section samples are given in the following sections and summarized in Table 2.

4.2 Microfacies description

4.2.1 MF1 (Microfacies 1) unit: fine sandstone to siltstone with basal erosion

At core scale, the MF1 unit mainly consists of sand and silt, with thickness of approximately 2–3 cm (Table 2). This unit also contains basal erosion surface, curved ripple lamina and low-angle cross bedding (Figs. 6a–f and Table 2). Based on thin section observation, the overall particle size is fine sand to silt (roughly 50–100 μm), and this microfacies has no significant upward grain size grading. In some samples, bioclasts are visible (Figs. 6g–h). At thin section scale, the basal erosion surface, curved ripple lamina and low-angle cross bedding remain visible. The basal erosion surface is submillimeter in scale (the erosion scour depth is approximately 0.1–1 mm) and has an angular form (Figs. 6g–f). The bottom boundary of the MF1 unit is an erosive contact, and the top boundary is a sharp contact (Fig. 6).

4.2.2 MF2 (Microfacies 2) unit: silt-streaked claystone

At core scale, the MF2 unit is mainly composed of interbedded silt- and clay-rich layers. The dominant sedimentary structure in the MF2 is wave ripple (Table 2). The MF2 unit drapes over MF1 and is influenced by its antecedent morphology at some locations (Figs. 7a-f). The silt- and clay-rich layers in the MF2 unit are parallel laminae with thicknesses approximately 1 mm (Figs. 7g–m). Based on thin section observation, the grain size of the silt-rich layers is approximately 20–50 μm (medium silt). The contact between the silt- and clay-rich layers is a sharp boundary at the thin section scale. Similarly, the top and bottom boundaries of the MF2 unit are also sharp contacts (Figs. 7g–j). In some samples, the interior of the silt-rich layers shows a fining upward grain size grade (Figs. 7k–m and Table 2).

4.2.3 MF3 (Microfacies 3) unit: silty-claystone

The MF3 unit is relatively uniform and structureless at core scale (Fig. 8). The thickness of MF3 units ranges from 0.5–3 cm (Table 2). There are some bioturbations developed near the boundaries or crosscut through the MF3 unit. The top and bottom boundaries of the MF3 unit are also sharp contacts (Figs. 8a-g). At thin section scale, the MF3 unit is mainly composed of clay particles, with very low silt content, and contains more bioturbation at

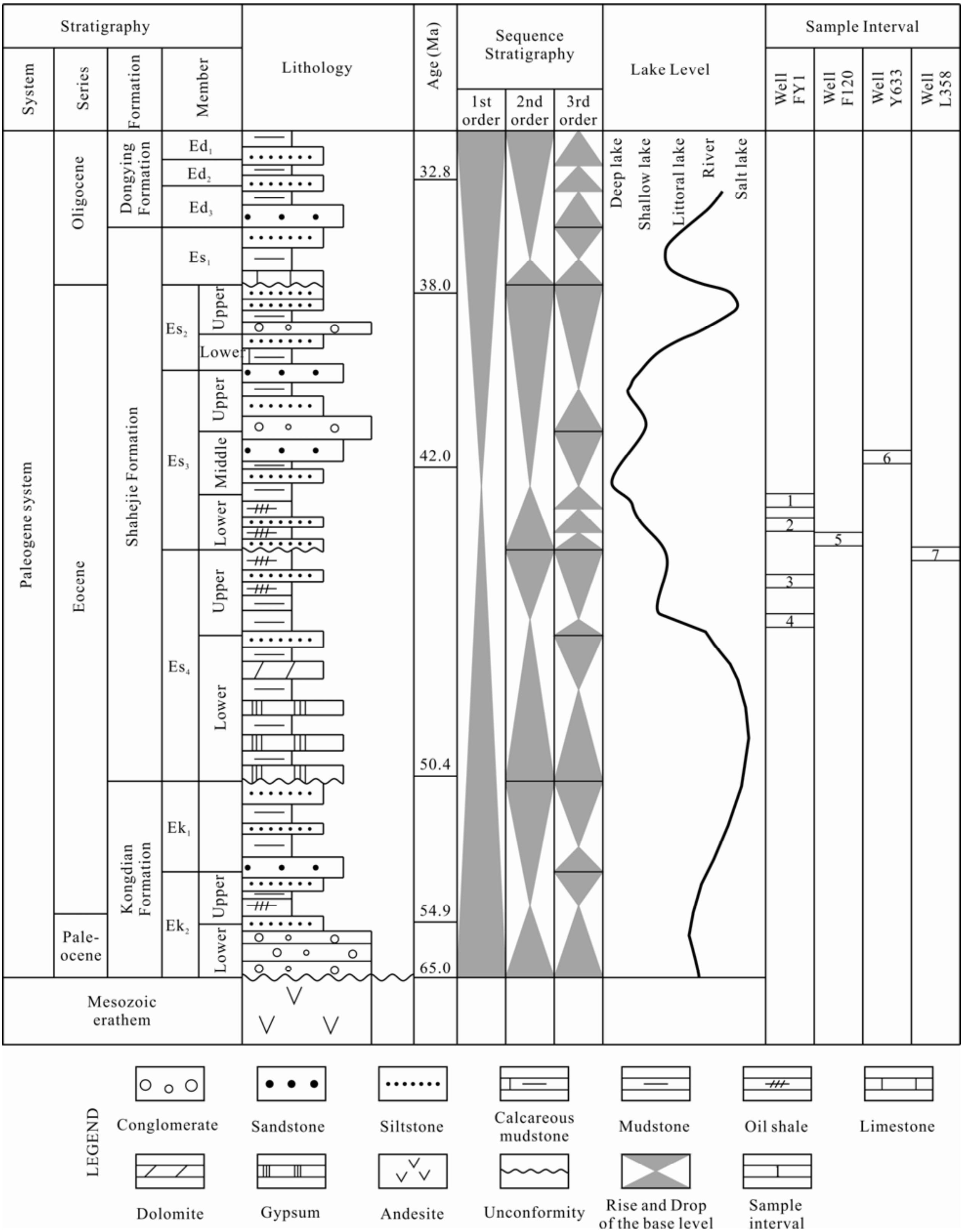

Fig. 3. The lithology and general sequence stratigraphic charts of the Jiyang sub-basin (modified from Feng et al., 2013 and Zahid et al., 2016).

The classification of different sequence order is based on Feng et al. (2013) and Zahid et al. (2016); lake level is based on Feng et al. (2013) and modified from detailed interpretation from this study. The ages of the sequence boundaries are derived from Feng et al. (2013). See Fig. 4 for detailed sample interval of wells FY1, F120, Y633 and L358.

the boundaries (Figs. 8h–l).

4.2.4 MFd (Microfacies delta) unit: clay-streaked siltstone

The MFd unit is very similar to the MF2 unit at core scale. Both units are composed of interbedded silt- and clay-rich layers with 0.4–1 mm thickness. However, detailed thin section observation indicates that the MFd unit is significantly different from the MF2 unit. The two boundary types (silt to clay, clay to silt) between the alternating clay- and silt-rich layers are a gradual and a sharp contact in the MFd unit (Table 2). In contrast, both boundaries are sharp in MF2. Moreover, sediment size coarsens upward between two adjacent sharp boundaries in MFd (Figs. 9e-f and Table 2).

5 Discussion

5.1 Hydrodynamic condition

The MF1 unit of the lacustrine WESGF sequences is mainly composed of silt and fine sand and does not contain the normal graded bedding structures that are observed in general gravity flow (Fukushima et al., 1985; Garcia and Parker, 1989). The millimeter-submillimeter-scale basal erosion surface of MF1 is different from that of the typical flute cast observed at base of turbidites (Sly et al., 2003; Kostic and Parker, 2006; Macquaker et al., 2010). This erosion surface also implies that the underlying layer is already consolidated (Macquaker et al., 2010; Plint, 2014). Therefore, there is a difference in formation mechanism between MF1 and a typical turbidity current. The main sedimentary structures of MF1 comprise curved ripple laminae, low-angle cross beddings, and some bioclastics. These structures are quite similar to marine WESGFs (Plint, 2014), which are interpreted to form in a relatively strong hydrodynamic environment. Low-angle cross bedding is likely to represent single directional fluid movement, such as a traction current (Macquaker et al. 2010). Furthermore, the curved ripple laminae possess a symmetrical form (Fig. 6), which is an evidence of orbital wave motion (Macquaker et al., 2010; Plint, 2014). Thus, the sedimentary structures of MF1 are produced by two types of flows, namely, traction current and wave action (Macquaker et al., 2010; Plint, 2014; Schieber, 2015) (Table 3).

MF2 consists of interbedded thin silt- and clay-rich layers. Silt- and clay-rich layers are generally parallel to the underlying MF1 unit, with sharp boundaries (Fig. 7). These structures imply that MF2 is formed under a sudden change from turbulent flow to laminar plug flow. According to the research of Baas and Best (2002), a silt-clay alternating structure typically forms due to turbulence

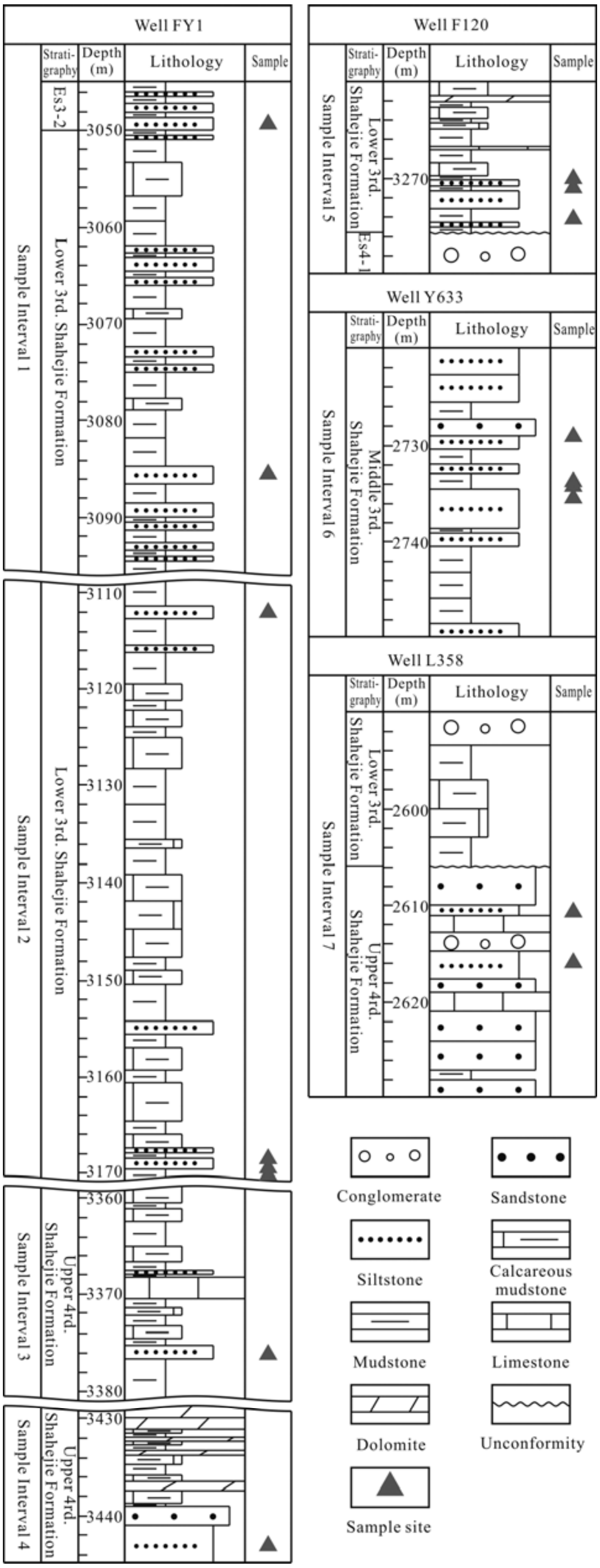

Fig. 4. The lithological column and sample site of well FY1, F120, Y633 and L358.

Sample intervals 1-4 belong to well FY1, sample interval 5 belongs to well F120, sample interval 6 belongs to well Y633, and sample interval 7 belongs to well L358.

caused by wave action. Such turbulence is eventually damped due to fluid density stratification and the flow gradually transitions to a laminar flow at the base (Table 3). MF2 tends to form at this change in flow state (Baas and Best, 2002; Plint, 2014). Because of this shift in hydrodynamic condition, there is an overall upward fining trend of MF2, with a gradual transition from silt to clay at the top boundary.

MF3 is a set of structureless mudstone (Fig. 8). The formation of MF3 is interpreted as a state in which the wave energy is not sufficient to produce adequate turbulence to maintain sediment in suspension. As the flow ceases, suspended sediments precipitate out from the water column and deposit uniformly over the MF2 unit. There are significantly more bioturbations developed in MF3 than in any other unit, implying a quiet environment after strong wave or storm events, which permitted burrowing organisms to thrive (Macquaker et al., 2010; Plint, 2014) (Table 3).

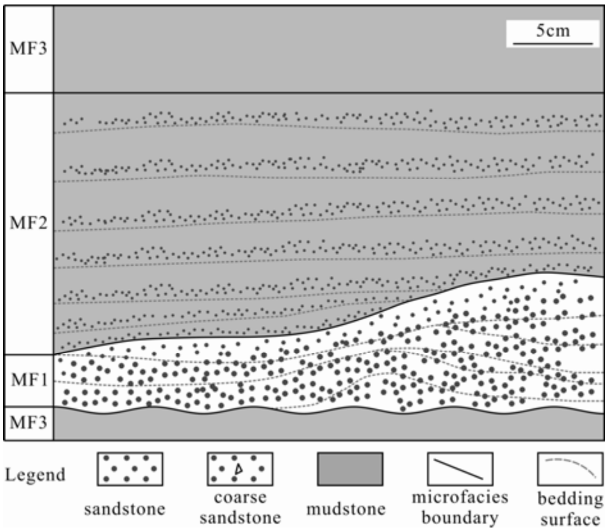

Fig. 5. Sketch of sedimentary units in lacustrine WESGFs (modified from Macquaker, et al., 2010 and Denommee, et al., 2016).

Table 1 The depth of samples

Wells	Depth (m)	Lithology
FY1	3049.10	Siltstone
FY1	3086.04	Siltstone
FY1	3112.00	Siltstone
FY1	3169.44	Sandstone/siltstone
FY1	3169.53	Sandstone/siltstone
FY1	3169.96	Siltstone
FY1	3376.64	Siltstone/claystone
FY1	3443.59	Sandstone/siltstone
F120	3270.10	Siltstone
F120	3270.83	Siltstone
F120	3274.80	Siltstone
Y633	2729.45	Sandstone/siltstone
Y633	2734.30	Siltstone
Y633	2734.35	Siltstone
Y633	2735.70	Siltstone/claystone
L358	2610.87	Sandstone/siltstone
L358	2616.28	Siltstone

It is difficult to distinguish the MFd and MF2 units based on core scale sedimentary structures. However, in the thin section scale, the contact between clay- to silt-rich layers in the MFd unit is a gradational boundary, and the contact between silt- to clay-rich layers is a sharp boundary. Between two adjacent sharp boundaries, grain size shows an upward coarsening trend in MFd unit. This type of grain size trend is generally observed in the sand sheet sequences produced near the distal end of prodelta facies (Etienne et al., 2012; Forman et al., 2014) or in sequences produced by hyperpycnal flow (Mulder et al., 2002). At both core and thin section scale, climbing ripples, which are an indicative characteristic of hyperpycnal flows (Mulder et al., 2002), are very rare in the samples. The abundance of bioturbations in the MFd unit also does not support the interpretation of hyperpycnal flows (Mulder et al., 2002). Therefore, the MFd unit is more likely to be classified as prodelta sand sheet (Table 3). Regardless of the mechanism, the MFd unit appears to have formed under a different hydrodynamic condition than the MF2 unit.

5.2 Microfacies sequence

The microfacies sequence of the lacustrine WESGF deposits in the study area has a general order, from bottom to top, as MF1-MF2-MF3 (Fig. 10), which is similar to that of marine WESGF sequences (Macquaker et al., 2010). The bottom units of both marine and lacustrine WESGF sequences contain basal erosion surface, curved ripple laminae and low-angle cross bedding. The ripples are symmetrical, indicating the effects of wave action. The middle units of both sequences are composed of silt- and clay-rich layers with sharp contacts. The top units are both composed of clay particles with no significant sedimentary structures. Hence, based on interpreted hydrodynamic condition, these sequences that appear in a lacustrine basin should be generated by WESGFs.

Occasionally, the sequence lacks an MF3 unit and only contains, from bottom to top, MF1-MF2 units (Fig. 10). The interpretation is that the wave energy increased

Table 2 The characteristics of WESGFs units

Units	Component	Thickness	Sedimentary Structure	Grain size grade
MF1	Sand and silt	2–3 cm	Basal ersion surface, curved ripple lamina and low-angle cross bedding	No grain size grade
MF2	Silt and clay	1 cm	Parallel lamina	Fining upward grain size grade
MF3	clay	0.5–3 cm	Structureless	No grain size grade
MFd	Silt and clay	1 cm or more	Parallel lamina	Coarsens upward grain size grade

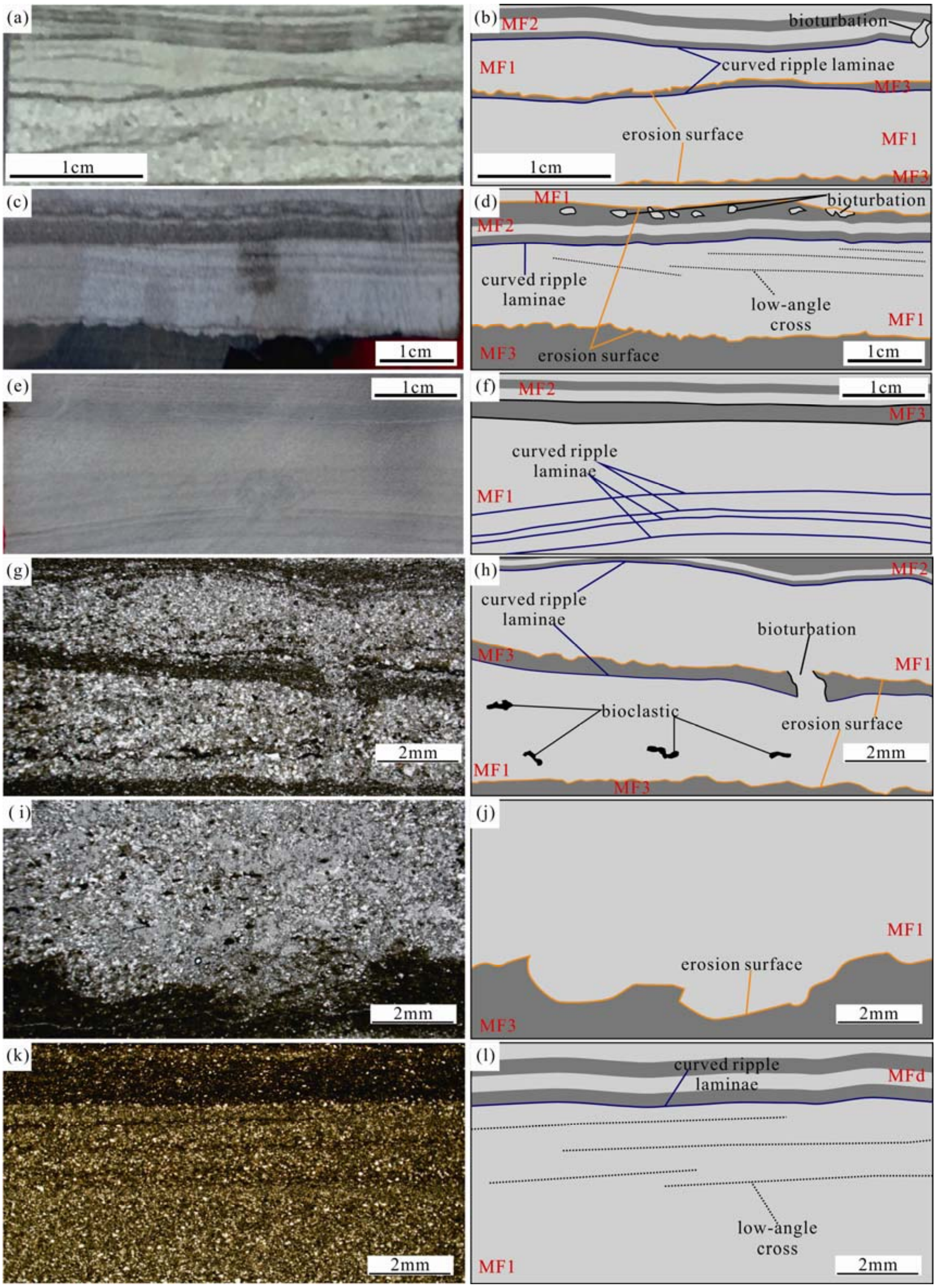

Fig. 6. The identifying characteristics of MF1.

(a), Well Y633, 2729.45 m, core photo; (b), interpretation of photo a, with visible curved ripple lamina and basal erosion surface indicative of MF1, bioturbation appears at the boundary of MF1 and MF2; (c), well FY1, 3169.44 m, core photo; (d), the interpretation of photo c, with visible curved ripple lamina, low-angle cross bedding and basal erosion surface indicative of MF1, several bioturbations appears at the boundary of MF1 and MF2; (e), well FY1, 3443.59 m, core photo; (f), interpretation of image e, with visible curved ripple lamina; in core photo, MF1 unit has clear sub-millimeter scale basal erosion surfaces (the thickness of erosion range is roughly 0.1–1 mm). Top boundaries of MF1 to MF2/MF3 are sharp contacts. (g), well Y633, 2729.45 m, thin section photo, taken under plane-polarized light; (h), interpretation of photo g, with visible curved ripple lamina and basal erosion surface, some carbon-rich bioclastic appear in MF1, and a bioturbation cut through the MF3; (i), well L358, 2610.87 m, thin section photo, taken under plane-polarized light; (j), the interpretation image of photo i, with visible basal erosion surface remarkably; (k), well FY1, 3169.44 m, thin section photo, taken under plane-polarized light; (l), interpretation of photo k, with visible curved ripple lamina and low-cross bedding; in thin section photo, the MF1 also have clear sub-millimeter scale basal erosion surfaces and top boundaries to MF2 (MFd)/MF3 are also sharp boundaries, the diameter of sand grains in MF1 are 50–100 μm roughly.

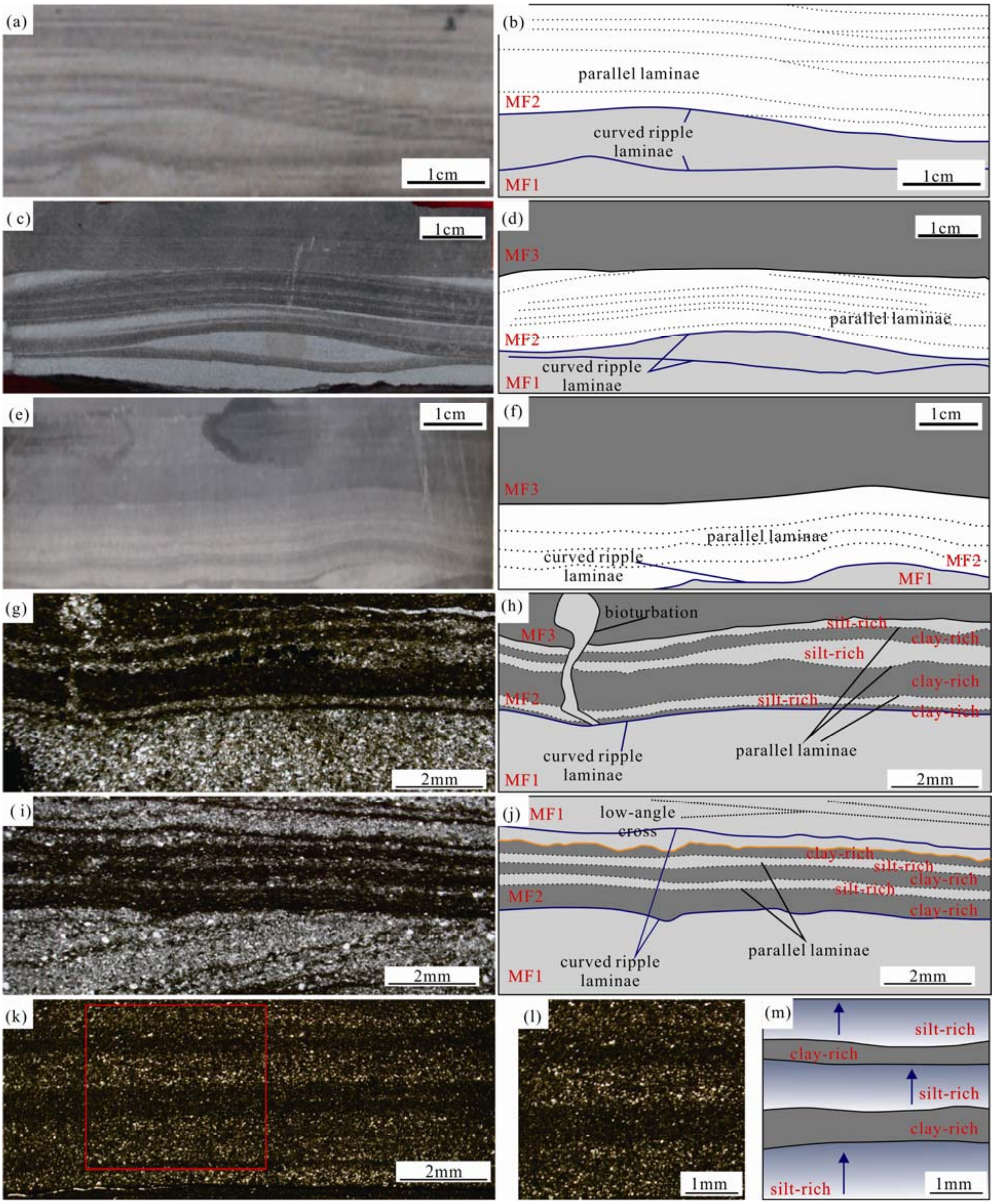

Fig. 7. The identifying characteristics of MF2.

(a), Well FY1, 3086.04 m, core photo; (b), the interpretation of photo a, with visible interbedded silt and mud layers, parallel lamina appears in MF2; (c), well FY1, 3169.96 m, core photo; (d), the interpretation of photo c, with visible interbedded silt and mud layers, parallel lamina appears in MF2; (e), well F120, 3270.10 m, core photo; (f), the interpretation of photo e, with visible interbedded silt and mud layers, parallel lamina appears in MF2; in core photo, the MF2 have sub-millimeter scale interbedded silt and mud layers, and have perfect parallel lamina commonly; (g), well L358, 2616.28 m, thin section photo, taken under plane-polarized light; (h), the interpretation image of photo g, clear interbedded silt-rich and clay-rich layers, also have parallel laminae, bioturbation cut through the whole MF2; (i), well Y633, 2734.30 m, thin section photo, taken under plane-polarized light; (j), the interpretation image of photo i, clear interbedded silt-rich and clay-rich layers, also have parallel laminae; (k), well FY1, 3443.59 m, thin section photo, taken under plane-polarized light; (l), enlarge of the red box in photo k, the thickness of silt-rich and clay-rich layers are about 1 mm; (m), the interpretation image of photo l, the boundaries of silt-rich and clay-rich layers are sharp boundaries, and the silt-layers show a fining upward succession; in thin section photo, the silt-rich and clay-rich layers are millimeter or sub-millimeter normally, the diameter of silt grains are 20–50 μm roughly.

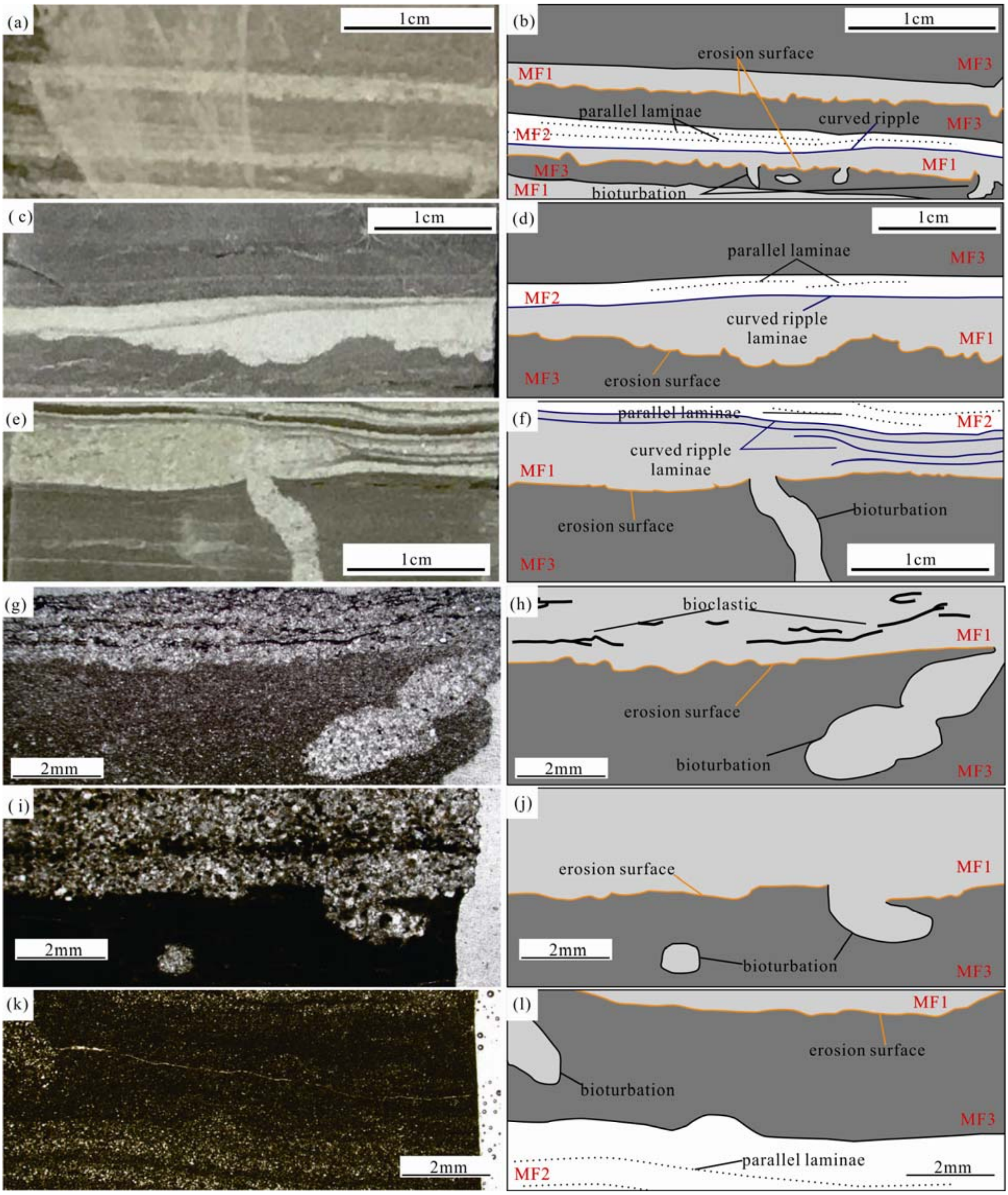

Fig. 8. The identifying characteristics of MF3.

(a), Well L358, 2610.87 m, core photo; (b), the interpretation image of photo a, the MF3 with homogeneous appearance and lacking dispersed silt grains, and some bioturbation appear in MF3; (c), well Y633, 2735.70 m, core photo; (d), the interpretation image of photo c, the MF3 with homogeneous appearance and lacking dispersed silt grains; (e), well Y633, 2734.30 m, core photo; (f), the interpretation image of photo e, the MF3 with homogeneous appearance and lacking dispersed silt grains, and some bioturbation appear in MF3; in core photo, the MF3 is mainly composed with clay minerals, have massive structure and bioturbation normally. (g), well Y633, 2735.70 m, thin section photo, taken under plane-polarized light; (h), the interpretation image of photo g, MF1 erosively overlying MF3, and bioturbation appear in MF3; (i), well L358, 2610.87 m, thin section photo, taken under plane-polarized light; (j), the interpretation image of photo i, MF1 erosively overlying MF3, and bioturbation appear in MF3; (k), well FY1, 3376.64 m, thin section photo, taken under plane-polarized light; (l), the interpretation image of photo k, MF3 sharply overlying MF2, and bioturbation appear in MF3; in thin section photo, part of thin sections visible see a few silt grains dispersed in MF3, and the diameter of these silt grains are less than 20 μm roughly.

periodically and maintained sufficient turbulence to keep the sediment in suspension. As a result, the hydrodynamic condition after the formation of MF2 unit does not allow sediment settling to form the MF3 unit. There is also a more distinct microfacies, MFd, which is interpreted as a prodelta sand sheet. It is speculated to form at low lake levels or during a period of high sediment supply, when the prodelta sand sheet is transported farther offshore and is preserved as MFd units within the overall WESGF sequences. The thickness of the individual lacustrine WESGFs sequences (MF1-MF2-MF3 or MF1-MF2) are roughly 3–10 cm; several WESGFs sequences are overlay in vertically, and those are roughly 5–30cm (Fig. 10).

5.3 Transport model of lacustrine WESGFs

The southern margin of the Boxing and Bonan sags contain classical prograding delta sequences (Guo et al., 2010; Feng et al., 2013; Wang et al., 2015). The delta plain deposits are composed of coarse sandstone, and its grain size fines downstream towards the shoreline. The system then transitions from fine-grained sandstone to siltstone of a prodelta environment (Fig. 11a), which is the potential source area and origin of the WESGFs. Some of these unconsolidated prodelta sands and muds are thought to travel to the lake center via WESGFs (Macquaker et al., 2010; Plint, 2014).

The orbital motion of the wave generates sufficient turbulence to resuspend prodelta sand and mud to initiate the WESGFs. As the flow travels down the southern lake slope, it erodes into the consolidated basement rock and forms an erosion surface. The body of the flow contains low-angle cross bedding and symmetrical ripple from wave motion, which forms the MF1 unit (Fig. 11b). As the head of the WESGFs passes, the tail of the flow is influenced by wave action and forms the interbedded clay and silt layer of MF2, as the flow transitions from turbulent to laminar due to Kelvin-Helmholtz instabilities (Baas and Best, 2002). At the end of the event, the flow travels to a depth below the wave base. In this case, the wave energy disappears, and the slope is too shallow to provide adequate gravitational force to maintain WESGFs in motion. The sediment then settles and forms the MF3 unit through electrostatic gelling (Macquaker et al., 2010; Plint, 2014). Sometimes, if the wave energy becomes too strong or the wave base deepens, then the sediment does not settle, and the flow continues toward the deep lake area; thus, the MF3 unit does not form. Since the WESGFs form close to the prodelta margin, delta progradation should allow the incorporation of deltaic deposits (i.e., prodelta sand sheet) into the WESGFs sequence as MFd units (Fig. 11c).

5.4 The differences between lacustrine and marine WESGFs and other sediment-gravity flows

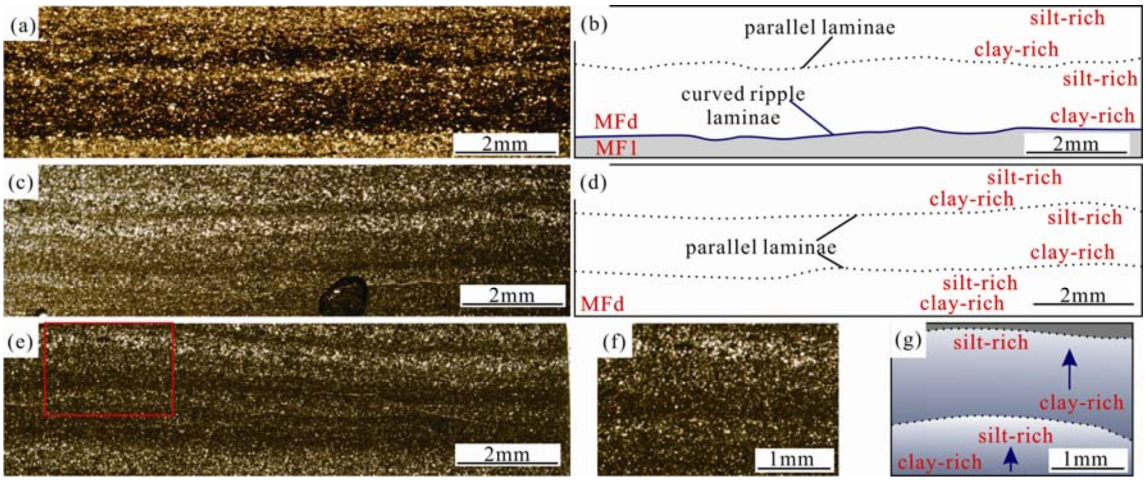

Fig. 9. The microscopic structure of MFd.
(a), Well Y633, 2734.35 m, thin section photo, taken under plane-polarized light; (b), the interpretation image of photo a, the MFd is also composed by silt-rich and clay-rich layers, and have parallel laminae; (c), well F120, 3274.80 m, thin section photo, taken under plane-polarized light; (d), the interpretation image of photo c, the MFd is also composed by silt-rich and clay-rich layers, and have parallel laminae; (e), well FY1, 3443.59 m, thin section photo, taken under plane-polarized light; (f), enlarge of the red box in photo e, the thickness of silt-rich and clay-rich layers are about 1 mm; (g), the interpretation image of photo f, from clay-rich layer to silt-rich layer is gradational boundaries, from silt-rich layer to clay-rich layer is sharp boundaries, and from clay-rich to silt-rich layers show a coarsening succession.

Table 3 The hydrodynamic and control factors of WESGFs units

Units	Hydrodynamic condition	Control factors
MF1	Strong	Traction current and wave action
MF2	Middle	Sudden change from turbulent flow to laminar plug flow
MF3	Weak	Electrostatic gelling
MFd	Weak	Hyperpycnal flows or prodelta sand sheet

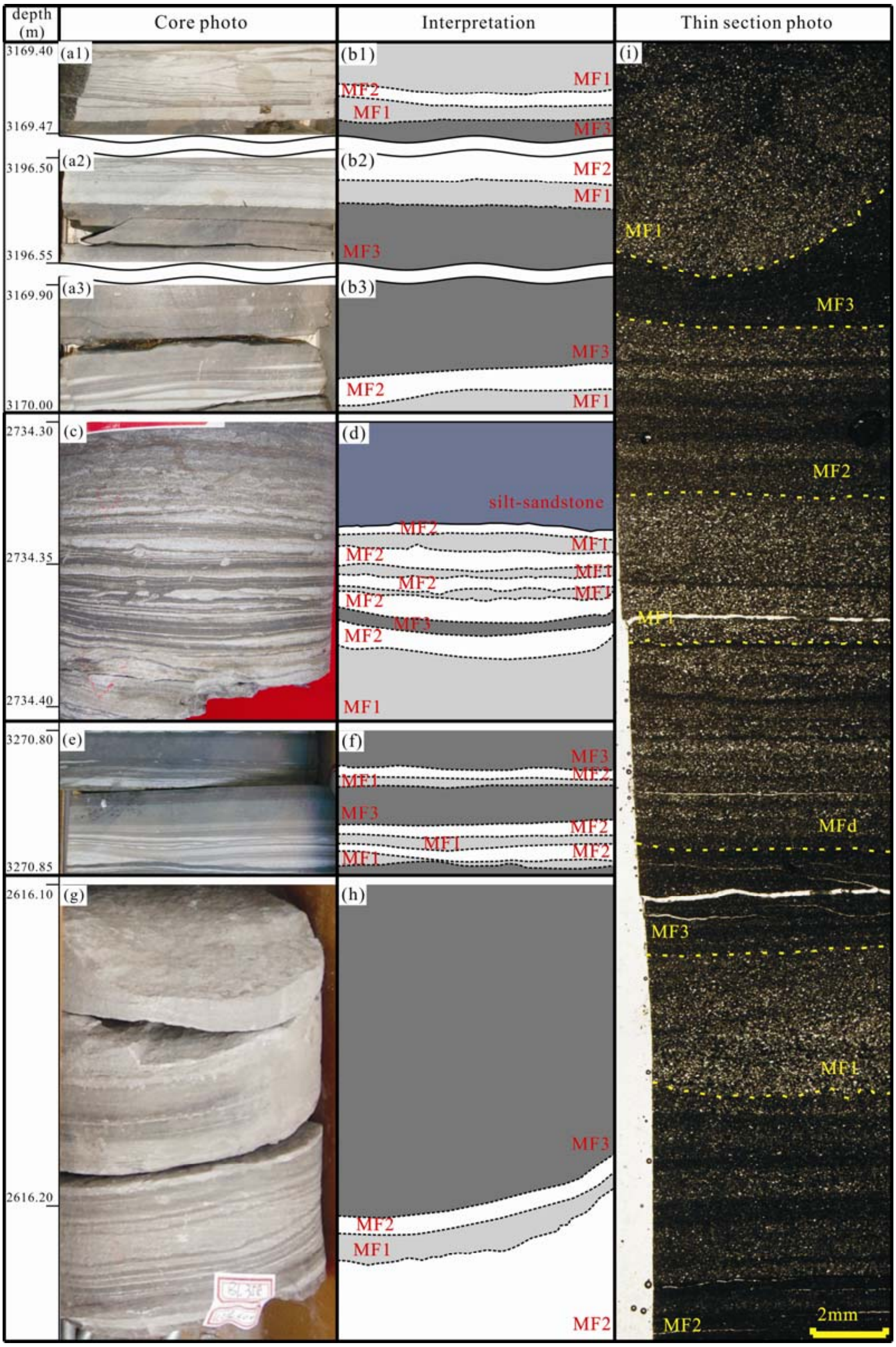

Fig. 10. The microfacies combine of WESGFs.

(a), The core photo of well FY1, (a1) 3169.40~3169.47 m, (a2) 3169.50~3169.55m, (a3) 3169.90~3170.00 m; (b), the interpretation image of photo a, (b1) the bottom part is MF3, and the sequence overlying MF3 is MF1-MF2-MF1 (lack MF3); (b2) the bottom part is MF3, and the sequence overlying MF3 is MF1-MF2; (b3) bottom to top is complete sequence MF1-MF2-MF3; (c), the core photo of well Y633, 2734.30~2734.40 m; (d), the interpretation image of photo c, the bottom part is complete sequence MF1-MF2-MF3, the middle part is several MF2-MF1 sequences (lack MF3), the top part is siltstone and sandstone; (e), the core photo of well F120, 3270.90~3270.85 m; (f), the interpretation image of photo e, the bottom part is MF1-MF2 sequence (lack MF3), the middle and top part are two complete sequences MF1-MF2-MF3; (g), the core photo of well L358, 2616.10~2616.20 m; (h), the interpretation image of photo g, the bottom part is MF2, and a complete sequence overlying the MF2; (i), the thin section image of FY1, 3443.59 m, under plane-polarized light, vertical section of microfacies, yellow dashed lines indicated microfacies boundary, bottom part is MF2 unit, middle part is MFd unit, top part is unit, under MFd unit is MF1-MF3 sequence, upon MFd is complete sequence MF1-MF2-MF3.

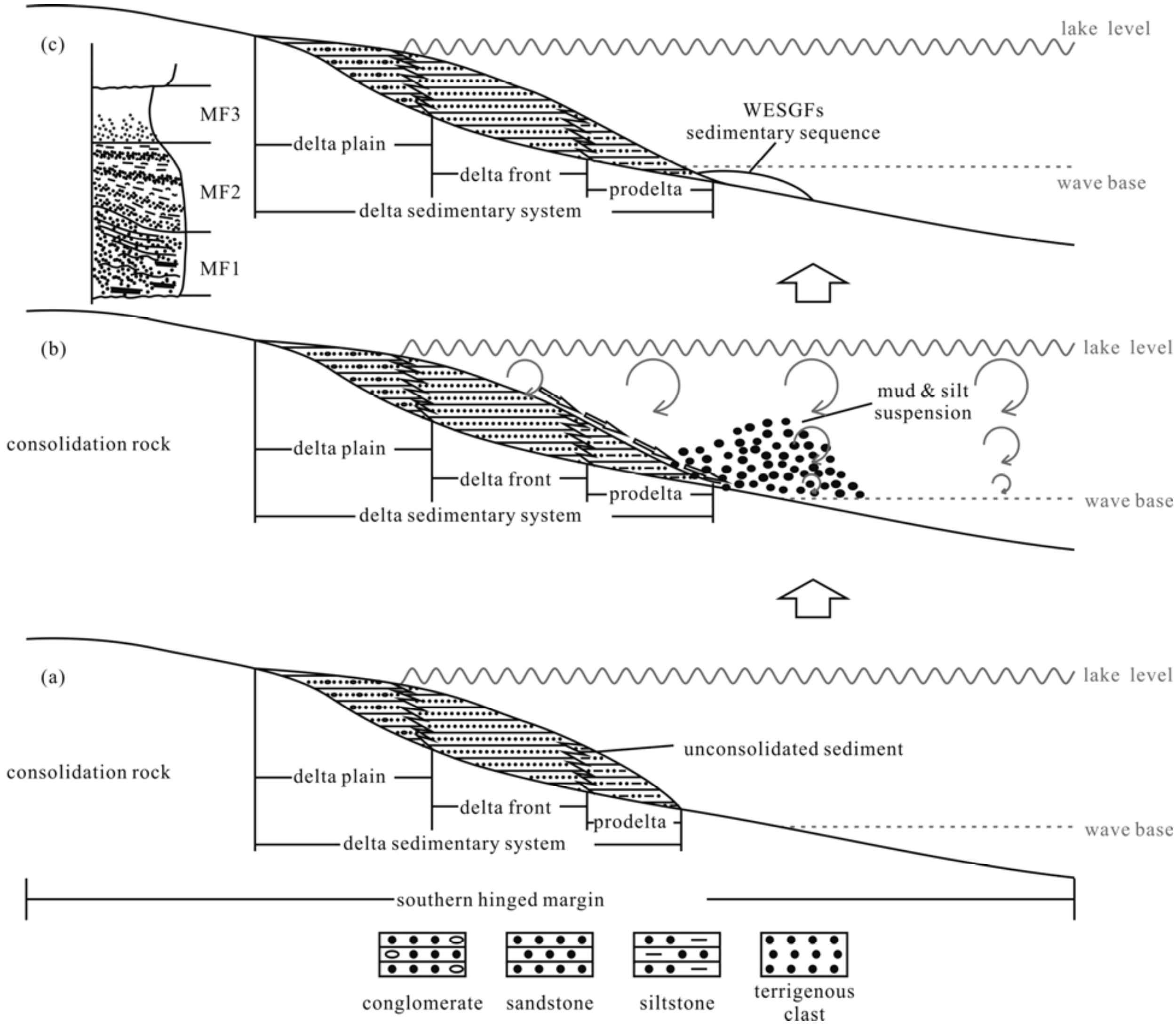

Fig. 11. Evolution pattern of lacustrine WESGFs sequence.

(a), The delta sedimentary system appear in the hinged (gentle slope) margin of lacustrine basin, and the sand and mud sediments deposited on the delta front and prodelta; (b), the sand and mud sediments resuspension with wave action, and form the turbulent flow, this turbulent flow transports the sediments to offshore direction along the gentle slope margin of lacustrine basin (form MF1); (c), with sediment concentrations increase and the flow inter to deeper water environment, the energy of the wave is attenuation rapidly, turbulence is dampened, an abrupt change in flow regime (form MF2); at the end of the succession, the wave energy is unable to keep the flow moving, through electrostatic gelling of the flow form the MF3.

There are some differences between marine and lacustrine WESGFs due to the difference in system size and to additional flows in ocean. In a lacustrine WESGFs sequence, the sedimentary structures, e.g., ripple laminae, are smaller than those of the marine sequences. Lacustrine WESGFs sequences in this study only contain 1–4 complete/incomplete stacks with a total thickness of 5–30 cm, which are much less than those of the marine sequences. The sand/silt fraction and grain size in the lacustrine WESGFs sequence are higher than those of the marine sequence.

In a marine setting, waves can be generated from gravity, tides, wind and storms, all of which contain a particular pattern of cyclicality (Baumann et al., 2017; Mao and Xia, 2017; Prather et al., 2017). Meanwhile, the waves in lakes are mainly generated by wind derived from the local pressure regime, and they have a less cyclical pattern. Microclimates in the lake environment change rapidly, which can potentially reduce wind and wave energy (Gilbert, 1999; Immenhauser, 2009; Mao and Xia, 2017). As a result, the sedimentary structures of lacustrine WESGFs are smaller than those of the marine WESGFs.

As description above and some previously researches in study area, with adequate sediment supply and appropriate triggering mechanisms, study area allow other types of sediment-gravity flows, such as hyperpycnal flow and turbidity current, to form. However, the observed sedimentary structures and microfacies sequences in this study are more indicative of WESGFs. For example, compared to hyperpycnal flow, the microfacies of this study contain many more bioturbations (MF3 unit) (Mulder et al., 2002). Furthermore, the sharp boundaries between silt- and clay-rich laminae of the MF2 unit are different, which are attributable to an accelerating and decelerating hyperpycnal flow (Mulder et al., 2002). Finally, the scale of the studied sequence is different, i.e., both the transport distance and sizes of the sedimentary structures are much smaller than those of sequences formed by hyperpycnal flow (Mulder et al., 2002; Yang Tian et al., 2017). In comparison with turbidite sequences, the bottom unit of the WESGFs sequences contain millimeter-scale erosion surfaces (0.1–1 mm scour depth), which are different from those of the flute cast at the base of typical turbidite sequences (Bouma, 2000; Postma et al., 2015; Wang et al., 2017). Additionally, the sediment grain size of the lacustrine WESGFs deposits is much finer than the coarse sand and gravel grains at the base of typical turbidites (Bouma, 2000; Postma et al., 2015). Moreover, the structure of MF2 unit, parallel silt- and clay -rich laminae with sharp boundaries, is very different than that of the Tb (sandstone with parallel bedding and transition boundaries) or Td (siltstone with horizontal bedding and transition boundaries) unit of the Bouma sequence (Bouma, 2000; Postma et al., 2015). Furthermore, a turbidity current normally forms in submarine canyon or other steep slope regions (Bouma, 2000; Postma et al., 2015; Wang et al., 2017); however, in this study, the WESGFs were formed slightly offshore of the prodelta region. Overall, the observed microfacies and associated depositional setting are not indicative of a common turbidity current. Instead, based on the above analysis, the studied sequences are more likely to have been formed by WESGFs.

6 Conclusion

(1) This research utilized core samples and thin section data from the Jiyang sub-basin, eastern China to characterize a set of sedimentary sequences in a lacustrine environment. Based on the core observation and microstructure analysis, the sedimentary sequences are interpreted to have been formed by WESGFs. Thus, in addition to the marine environment, WESGFs can also form in a lacustrine basin.

(2) The lacustrine WESGFs can be divided into three units, MF1 unit: siltstone with basal erosion, MF2 unit: silt -streaked claystone, and MF3 unit: silty-mudstone. Moreover, the lacustrine WESGFs have a unique MFd unit: clay-streaked siltstone. This unit potentially forms due to the proximity of lacustrine WESGFs to a prodelta system, which can incorporate some delta sequences.

(3) Due to the differences in system scale and in the variability of hydrodynamic conditions between lacustrine and marine basins, the lacustrine WESGFs have some distinctive features as follow: the sediment grain size and sand content of lacustrine WESGFs are slightly higher than those of the marine WESGFs; this difference is due to the proximity to the delta system; the lacustrine WESGFs may incorporate some other flow regime sedimentary sequences, such as hyperpycnal flow; and the sedimentary structures of lacustrine WESGFs are smaller than those of the marine WESGFs.

(4) This research provides a new example of WESGFs deposits in the rock record. However, most importantly, the WESGFs found in a continental lake in this study provide a new model to explain sediment transport mechanisms in a lacustrine basin. This newly developed lacustrine WESGFs model can be used to help interpret and predict the distribution of sand bodies in lacustrine basins.

Acknowledgments

This research is made possible by the help of Sino Petroleum Corporation (SINOPEC) Shengli Oilfield. Much thanks to State Key Laboratory of Geological Processes and Mineral Resources, China University of Geosciences for preparing the thin sections. This research is support by the National Nature Science Foundation of China (General Program) Grant No. 41572134 and National Program on Key Basic Research Project of China (973 Program) Grant No. 2014CB239102.

Manuscript received Dec. 26, 2017
accepted Jul. 27, 2018
edited by Li Lian

References

Baas, J.H., and Best, J.L., 2002. Turbulence Modulation in Clay-Rich Sediment-Laden Flows and Some Implications for Sediment Deposition. *Journal of Sedimentary Research*, 72 (3): 336–340.

Bai, C., Yu, B., Liu, H., Xie, Z., Han, S., Zhang, L., Ye, R., and Ge, J., 2018. The genesis and evolution of carbonate minerals in shale oil formations from Dongying depression, Bohai Bay Basin, China. *International Journal of Coal Geology*, 189: 8–26.

Baumann, J., Chaumillon, E., Schneider, J.L., Jorissen, F., Sauriau, P.G., Richard, P., Bonnin, J., and Schmidt, S., 2017. Contrasting sediment records of marine submersion events related to wave exposure, Southwest France. *Sedimentary Geology*, 353: 158–170.

Bouma, A.H., 2000. Coarse-grained and fine-grained turbidite systems as end member models: applicability and dangers. *Marine and Petroleum Geology*, 17(2): 137–143.

Clayer, F., and Desrochers, A., 2014. The stratigraphic imprint of a mid-Telychian (Llandovery, Early Silurian) glaciation on far

-field shallow-water carbonates, Anticosti Island, Eastern Canada. *Estonian Journal of Earth Sciences*, 63(4): 207–213.

Denommee, K.C., Bentley, S.J., Harazim, D., and Macquaker, J.H.S., 2016. Hydrodynamic Controls on Muddy Sedimentary -Fabric Development on the Southwest Louisiana Subaqueous Delta. *Marine Geology*, 382: 162–175.

Etienne, S., Mulder, T., Bez, M., Desaubliaux, G., Kwasniewski, A., Parize, O., Dujoncquoy, and E., Salles, T., 2012. Multiple scale characterization of sand-rich distal lobe deposit variability: Examples from the Annot Sandstones Formation, Eocene–Oligocene, SE France. *Sedimentary Geology*, 273–274: 1–18.

Feng, Y.L., Li, S.T., and Lu, Y.C., 2013. Sequence stratigraphy and architectural variability in Late Eocene lacustrine strata of the Dongying Depression, Bohai Bay Basin, Eastern China. *Sedimentary Geology*, 295: 1–26.

Forman, S.L., Tripaldi, A., and Ciccioli, P.L., 2014. Eolian sand sheet deposition in the San Luis paleodune field, western Argentina as an indicator of a semi-arid environment through the Holocene. *Palaeogeography, Palaeoclimatology, Palaeoecology*, 411: 122–135.

Friedrichs, C.T., and Wright, L.D., 2004. Gravity-driven sediment transport on the continental shelf: implications for equilibrium profiles near river mouths. *Coastal Engineering*, 51(8–9): 795–811.

Fukushima, Y., Parker, G., and Pantin, H.M., 1985. Prediction of ignitive turbidity currents in Scripps Submarine Canyon. *Marine Geology*, 67(1–2): 55–81.

Garcia, M., and Parker, G., 1989. Experiments on Hydraulic Jumps in Turbidity Currents near a Canyon-Fan Transition. *Science*, 245(4916): 393–396.

Ghadeer, S.G., and Macquaker, J.H.S., 2012. The role of event beds in the preservation of organic carbon in fine-grained sediments: Analyses of the sedimentological processes operating during deposition of the Whitby Mudstone Formation (Toarcian, Lower Jurassic) preserved in northeast England. *Marine and Petroleum Geology*, 35(1): 309–320.

Gilbert, R., 1999. Calculated Wave Base in Relation to the Observed Patterns of Sediment Deposition in Northeastern Lake Ontario. *Journal of Great Lakes Research*, 25(4): 883–891.

Guo, X.W., He, S., Liu, K.Y., Song, G.Q., Wang, X.J., and Shi, Z.S., 2010. Oil generation as the dominant overpressure mechanism in the Cenozoic Dongying depression, Bohai Bay Basin, China. *AAPG Bulletin*, 94(12): 1859–1881.

Guo, X. W., Liu, K. Y., He, S., Song, G. Q., Wang, Y. S., and Hao, X. F., 2012. Petroleum generation and charge history of the northern dongying depression, Bohai Bay basin, China: insight from integrated fluid inclusion analysis and basin modelling. *Marine and Petroleum Geology*, 21(4), 21–35.

Hao, Y., Chen, F., Zhu, J., and Zhang, S., 2014. Reservoir space of the Es_3^3–Es_4^1 shale in Dongying sag. *International Journal of Mining Science and Technology*, 24(4): 425–431.

Harazim, D., and Mcilroy, D., 2015. Mud-Rich Density-Driven Flows along an Early Ordovician Storm-Dominated Shoreline: Implications for Shallow-Marine Facies Models. *Journal of Sedimentary Research*, 85(5): 509–528.

Immenhauser, A., 2009. Estimating paleo-water depth from the physical rock record. *Earth Science Reviews*, 96(1): 107–139.

Kostic, S., and Parker, G., 2006. The response of turbidity currents to a canyon–fan transition: internal hydraulic jumps and depositional signatures. *Journal of Hydraulic Research*, 44(5): 631–653.

Lv Qiqi, Luo Shunshe, Fu Jinhua, Xiang Ji, Niu Xiaobing, Gong Chen, Xu Liming, Feng Shengbin and Li Shixiang, 2017. Outcrop-based analysis of a deep-water gravity flow sediments in lake: a case study from the chang 7 of yaoqu section, ordos basin. *Acta Geologica Sinica*, 91(3): 617–628 (in Chinese with English abstract).

Macquaker, J.H.S., Bentley, S.J., and Bohacs, K.M., 2010. Wave -enhanced sediment-gravity flows and mud dispersal across continental shelves: Reappraising sediment transport processes operating in ancient mudstone successions. *Geology*, 38(10): 947–950.

Mao, M., and Xia, M., 2017. Dynamics of wave–current–surge interactions in Lake Michigan: a model comparison. *Ocean Modelling*, 110: 1–20.

Mulder, T., Migeon, S., Savoye, B., and Faugères, J.C., 2002. Reply to discussion by Shanmugam on Mulder et al. (2001, Geo-Marine Letters 21: 86–93) Inversely graded turbidite sequences in the deep Mediterranean. A record of deposits from flood-generated turbidity currents? *Geo-Marine Letters*, 22(2): 112–120.

Nittrouer, C.A., and Wright, L.D., 1994. Transport of particles across continental shelves. *Reviews of Geophysics,* 32(1): 85–113.

Plint, A.G., 2014. Mud dispersal across a Cretaceous prodelta: Storm-generated, wave-enhanced sediment gravity flows inferred from mudstone microtexture and microfacies. *Sedimentology*, 61(3): 609–647.

Postma, G., Kleverlaan, K., and Cartigny, M.J.B., 2015. Recognition of cyclic steps in sandy and gravelly turbidite sequences, and consequences for the Bouma facies model. *Sedimentology*, 61(7): 2268–2290.

Prather, B.E., O'Byrne, C., Pirmez, C., and Sylvester, Z., 2017. Sediment partitioning, continental slopes and base of slope systems. *Basin Research*, 29(3): 394–416.

Schieber, J., 2015. Discussion: "Mud dispersal across a Cretaceous prodelta: Storm generated, wave-enhanced sediment gravity flows inferred from mudstone microtexture and microfacies" by Plint (2014), Sedimentology 61, 609–647. *Sedimentology*, 62(1): 389–393.

Sly, P.D., Cahill, P., Willet, K., and Burton, P., 2003. Reconstruction of turbidity currents in Amazon Channel. *Marine and Petroleum Geology*, 20(6–8): 823–849.

Tong Yanming, Han Fei, He Youbin and Peng Detang, 2008. Analysis based on GIS of sedimentary facies of the Member 3 of Paleogene Shahejie Formation in BonanSag,Bohai Bay Basin. *Journal of Palaeogeography*, 10(2): 215–220 (in Chinese with English abstract).

Traykovski, P., Wiberg, P.L., and Geyer, W.R., 2007. Observations and modeling of wave-supported sediment gravity flows on the Po prodelta and comparison to prior observations from the Eel shelf. *Continental Shelf Research*, 27(3): 375–399.

Walsh, J.P., Corbett, D.R., Kiker, J.M., Orpin, A.R., Hale, R.P., and Ogston, A.S., 2014. Spatial and temporal variability in sediment deposition and seabed character on the Waipaoa River margin, New Zealand. *Continental Shelf Research,* 86: 85–102.

Wang, J., Xie, X., Pang, X., and Liu, B., 2017. Storm-reworked shallow-marine fans in the Middle Triassic Baise area, South

China. *Sedimentary Geology*, 349: 33–45.

Wang Jian, Cao Yingchang, Song Guoqi and Liu Huimin, 2017. Diagenetic evolution and formation mechanisms of high-quality reservoirs under multiple diagenetic environmental constraints: an example from the paleogene beach-bar sandstone reservoirs in the Dongying depression, Bohai Bay basin. *Acta Geologica Sinica* (English Edition), 91(1), 232–248.

Wang, M., Wilkins, R.W.T., Song, G., Zhang, L., Xu, X., Li, Z., and Chen, G., 2015. Geochemical and geological characteristics of the Es3 L lacustrine shale in the Bonan sag, Bohai Bay Basin, China. *International Journal of Coal Geology,* 138: 16–29.

Yang Tian, Cao Yingchang and Wang Yanzhong, 2017. A new discovery of the early cretaceous supercritical hyperpycnal flow deposits on Lingshan Island, east China. *Acta Geologica Sinica* (English Edition), 91(2), 749–750.

Zahid, M.A., Dong, C., Lin, C., Gluyas, J., Jones, S., Zhang, X., Munawar, M.J., Ma, C., 2016. Sequence stratigraphy, sedimentary facies and reservoir quality of Es4s, southern slope of Dongying Depression, Bohai Bay Basin, East China. *Marine and Petroleum Geology*, 77: 448–470.

Zhang Shun, Liu Huimin, Chen Shiyue, Wang Yongshi, Pu Xiugang, Zhang Kuihua and Han Wenzhong, 2017. Classification scheme for lithofacies of fine-grained sedimentary rocks in faulted basins of eastern China: insights from the fine-grained sedimentary rocks in paleogene, southern Bohai Bay basin. *Acta Geologica Sinica*, 91(5): 1108–1119 (in Chinese with English abstract).

Zhu Xiaomin, Liu Fen, Tan Mingxuan, Han Xuefang, Zhang Shoupeng, Geng Mingyang, Li Wei and Dong Yanlei, 2015. Diagenesis and Genesis of Favorable Reservoir of Fan Delta in Eocene Shahejie Fm., Zhanhua Sag Jiyang Depression, Bohai Bay Basin. *Geological Review*, 61(4): 843–851 (in Chinese with English abstract).

About the first author

BAI Chenyang, male; born in 1991 in Zhuozhou City, Hebei Province; Ph. D. candidate in China University of Geosciences Beijing. He is research focuses on sedimentology and carbonate reservoir quality prediction. Email: cheny.bai@cugb.edu.cn; phone: 18618488331.